International Journal of Refrigeration 175 (2025) 164–173

Contents lists available at ScienceDirect

International Journal of Refrigeration

journal homepage: www.elsevier.com/locate/ijrefrig

INSTITUT INTERNATIONAL DU FROID
INTERNATIONAL INSTITUTE OF REFRIGERATION

Innovative photoacoustic instrument for fast and accurate detection and localization of R-134a leaks in refrigeration systems

Panna Végh [a,*], Bence Molnár [a], Máté Molnár [a], Piroska Ailer [a,c], Zoltán Bozóki [a,b], Helga Huszár [a,b]

[a] Department of Optics and Quantum Electronics, University of Szeged, 9 Dóm Square, Szeged 6720, Hungary
[b] HUN-REN-SZTE Research Group for Photoacoustic Monitoring of Environmental Processes, 9 Dóm Square, Szeged 6720, Hungary
[c] Centre of Excellence for Interdisciplinary Research, Development and Innovation of the University of Szeged, 13 Dugonics Square, Szeged 6720, Hungary

ARTICLE INFO

Keywords:
Photoacoustic spectroscopy
Leak detection
Refrigerant detection

ABSTRACT

Refrigerant leaks are a common issue that can seriously impact both the performance of refrigeration systems and the environment. The need for reliable and sensitive leak detection has become increasingly critical due to regulatory bans on refrigerants with a high global warming potential. A new potential option for detecting possible leaks in refrigeration installations is the development of a highly sensitive photoacoustic (PA) instrument, which allows for more accurate, faster and easier detection of leakage points in refrigeration equipment than currently commercially available equipment. This article reports on the development of a highly sensitive photoacoustic instrument for the detection and localization of R-134a leaks to identify leaks at rates as low as 1.2 g/year in refrigeration systems. The developed system includes a quantum cascade laser that operates around 10.3 μm with a maximum output power of 84 mW. It features a stainless steel photoacoustic cell with two 40 mm resonator tubes, each with a 3.5 mm inner diameter. This setup ensures the accurate detection of R-134a refrigerant leaks by targeting specific absorption lines. The fast response time, wide dynamic concentration range, and high sensitivity of the PA instrument make it a promising tool for refrigerant leak detection. The paper also discusses spectral interference from other environmental and refrigerant gases, such as water vapor, carbon dioxide, ammonia, methane, propane, and R-32. A detailed finite element model has been developed and implemented in COMSOL Multiphysics 6.2. The simulation results matched the experimental data, validating the accuracy of the PA system.

1. Introduction

Refrigerant leaks are a common problem that can seriously affect both the performance of refrigeration systems and the environment. In particular, the emission of hydrofluorocarbon refrigerants (HFCs) is increasing, mainly because they are widely used as replacements for chlorofluorocarbons (CFCs) and hydrochlorofluorocarbons (HCFCs), since the Montreal Protocol was agreed (Montzka et al., 2015). The R-134a (1,1,1,2-tetrafluoroethane, HFC-134a) refrigerant gas is the most common HFC in the atmosphere. Like all HFC refrigerants, R-134a has an ozone depletion potential (ODP) of 0. It also offers excellent chemical and thermal stability, is non-toxic, non-flammable and highly compatible with most materials. Applications include, among others, commercial refrigerators and small freezers, as well as automotive air conditioning and transport refrigeration. Despite its many benefits, R-134a is a potent greenhouse gas with a global warming potential (GWP) value of 1300 compared to CO_2 (IPCC, 2023). Its usage is tightly restricted due to the current European F-gas regulations, which impose limitations on the use of fluorinated refrigerants with high GWP. (Heredia-Aricapa et al., 2020).

The detection of hydrofluorocarbon refrigerants in the environment primarily relies on gas chromatography, semiconductor gas sensors, thermal conductivity, and infrared spectroscopy. Gas chromatography (GC) offers a wide variety of detection methods, including electron capture detection (ECD) (Rivett et al., 2003), and mass spectrometry (MS) (Montzka et al., 1996). They offer high precision, low detection limits, and the ability to measure a wide range of hydrocarbons. However, gas chromatography systems tend to be bulky, so they are not suitable for gas sensing on-site. Semiconductor gas sensors are smaller and have been commonly used due to their affordability and size (Chen

* Corresponding author.
E-mail address: vegh.panna@szte.hu (P. Végh).

https://doi.org/10.1016/j.ijrefrig.2025.04.003
Received 15 November 2024; Received in revised form 26 March 2025; Accepted 3 April 2025
Available online 3 April 2025

et al., 2020). However, they have quite poor gas selectivity, so the instrument might give false alarms to other components in the environment. Thermal conductivity sensors are simple to operate and have low maintenance requirements, but selectivity can be poor for refrigerants with similar thermal properties and they have low sensitivity (Panda et al., 2024). Sensors based on non-dispersive infrared (NDIR) spectroscopy have relatively low cost and high sensitivity (Chen et al., 2024). The limitations of the NDIR gas sensors are possible interferences, and they can be affected by changes in temperature and humidity, which may lead to inaccuracies if not properly compensated.

Photoacoustic spectroscopy (PAS) is one of the most sensitive methods for detecting trace gases because of its background-free absorption properties. In recent years, systems based on photoacoustic spectroscopy have been designed to detect refrigerant gases. Pereira and Melo (2019) developed "an experimental technique capable of identifying product deviations that affect the infiltration rate in refrigerated compartments". Their findings demonstrated high repeatability in measurements, with <5 % deviation, and confirmed the practicality of the method through tests on various refrigerators. El-Safoury et al. (2020) presented a three-chamber-based sensor concept to monitor the refrigerants R-134a and R-1234yf at higher concentrations. Their measurements were carried out with a gas mixture of R134a and N_2, where the concentration of R134a was changed in 20 vol. % increments from 0 to 100 vol. %. Qi et al. (2023) developed a photoacoustic detector for gaseous halocarbon refrigerants and extinguishing agents. This detector operates using a broadband source in the mid-infrared range, the gases targeted in their study were H-1301, R-134a, and R-410a.

Since the discovery of the photoacoustic effect, photoacoustic spectroscopy has made enormous progress, and while it has been in use for decades in various detector products, its further development continues to present significant opportunities for innovation and new applications. The photoacoustic concentration measurement technique is widely recognized for its exceptional selectivity, sensitivity, and accuracy in measuring concentrations. (Végh et al., 2024) Photoacoustic spectroscopy has several advantages, which are also very important for the localization of refrigerant leaks. One of the several attractive features of photoacoustic gas detection is the simple relation between the PA signal (defined as the microphone signal at the laser modulation frequency) and the concentration of the light-absorbing analyte. The magnitude of the photoacoustic signal is directly proportional to the concentration of the measured substance, so that the concentration can be calculated from the magnitude of the photoacoustic signal measured by the instrument. This is advantageous because in addition to determining the presence of the gas, it can also be used to determine the extent of it, as we can infer changes in the quantity based on the photoacoustic signal, and it can be used for source identification as the gas concentration is significantly higher near the leak points, resulting in signal peaks. Other advantages are that it has an exceptionally wide dynamic concentration range (5–6 orders of magnitude), i.e. from ppm (parts per million) to percent, and that even a small sample volume (a few cm^3) can be sufficient for the measurement, which allows a fast response time (1–2 s) to monitor the change in concentration. This is essential for refrigerant detection and source location identification. When the right light sources and measurement techniques are chosen, photoacoustic instruments provide selective measurement so that the instrument does not give false alarms to other components in the environment, as different components can absorb different wavelengths, so that individual refrigerants can be detected separately. The aim of the research presented here was to develop a highly sensitive instrument to identify possible R-134a leaks in refrigeration systems more accurately, faster, and easier than the methods currently used.

2. Theoretical section

2.1. Basics of photoacoustic theory

The PA signal is generated by modulated light whose wavelength coincides with the measured component absorption band. When molecules absorb light, they are excited to a higher energy state and can return to lower energy levels by three different mechanisms (Tam, 1986; Bozóki et al., 2011):

- Radiative relaxation, i.e. by emitting a photon.
- Colliding with another molecule causes the absorbed light energy to be converted into kinetic energy during collision.
- Colliding with another molecule, transferring the energy, therefore exciting this molecule.

The role of radiative relaxation is significant for low pressure gas samples and high photon energies (UV and visible range excitation), whereas for normal pressure and infrared excitation, nonradiative relaxation is dominant. In the second case, a photoacoustic signal is generated, and the third relaxation path may affect the generation of the photoacoustic signal. The excited molecules transfer excess energy to the surrounding molecules in the form of kinetic energy by collisions, so that their average velocity increases, which means an increase in temperature and an increase in pressure due to thermal expansion. If the excitation is periodic (which can occur with short light pulses or modulated light beams), then the temperature and pressure changes in the gas will also be periodic, i.e. the excitation will produce sound if modulated at acoustic frequency.

The principal equation of photoacoustics can be written in the following simplified form. For the sake of simplicity, the effect of possible spectral interference and non-instantaneous molecular relaxation is neglected.

$$PAS(f_r) = P_{\text{in}} \cdot M(f_r) \cdot C(f_r) \cdot \left(\alpha_{\text{spec}} \cdot c\right) + A_0(f_r). \quad (1)$$

In Equation (1), *PAS* (f_r) is the PA signal (in V) defined as the amplitude of the microphone output electric signal in the case when the laser modulation frequency is equal to the actual value of the resonance frequency of the PA cell (f_r in Hz). P_{in} is the light power of the laser going through the PA cell (in W), C is the cell constant (in $V \cdot cm \cdot W^{-1}$), M is the sensitivity of the measuring microphone which depends on the frequency (in $mV \bullet Pa^{-1}$), and α_{spec} is the specific optical absorption coefficient of the unit concentration of the measured component (in $cm^{-1} \cdot ppm^{-1}$), c is the concentration of the measured analyte (in ppm) and $A_0(f_r)$ is the background PA signal (in V) generated by light absorption on the walls and windows of the PA cell (i.e., it is the PA signal measured in case of zero analyte concentration). (Végh et al., 2024)

2.2. Requirements for detector sensitivity

Allowed by the F Gas Regulations (Regulation (EU) No. 573/2024) – the leak detector must have a sensitivity capable of detecting leaks at the maximum allowable rate of 5 g/year and should be checked annually.

Using the following relationship, one can convert a mass flow rate in the unit of g/s to $cm^3 \cdot min^{-1}$ (Goebel and Katz, 2008) and vice versa with

$$1\left[\frac{cm^3}{min}\right] = 7.43583 \cdot 10^{-7} \cdot M_a\left[\frac{g}{s}\right] \quad (2)$$

where M_a is mass of refrigerant in atomic mass units (AMU) (for example, 102 for R-134). Although the equation is valid at standard conditions of 0°C and pressure of 1013 hPa (1 atm), it can be used as an approximation for temperatures and pressures close to these conditions, with minimal error in practical applications.

2.3. Experimental section

The initial stage of the project involves the selection of the appropriate measurement wavelength. This requires the target of the refrigerant absorption lines, in which the concentration can be measured effectively, and spectral analysis to identify the spectral overlaps between different components, which can influence the photoacoustic signal. Afterward, it is necessary to select light sources with the required properties, such as output power, tuning range, and modulability. After the design and assembly of the laboratory prototype, the absorption lines will be meticulously measured, cross-effects examined, and calibrations and test measurements carried out.

2.4. Selection of the measuring wavelength, and cross-sensitivities

Fig. 1, 8, 18.

The most basic requirement for a light source is that it should have the same wavelength as the selected absorption line of the measured component. The most commonly used light sources in PA systems are distributed feedback (DFB) diode lasers, which operate in the near-IR wavelength range up to 2000 nm (Bozóki et al., 2011). However, the absorption lines of R-134a in the mid-IR region around 10 μm are significantly stronger than in the near-infrared (see Fig. 2), and hence a quantum cascade laser (QCL) emitting around 10.3 μm was chosen.

When selecting the measurement wavelength, it is crucial to consider what possible interference components might be present and relevant at various concentrations in the environment, even in exhaled air, such as water vapor, carbon dioxide, ammonia, and methane (see Fig. 3). The absorption spectra in Figs. 2 and 3 are based on The PNNL (Pacific Northwest National Laboratory) database, which provides a comprehensive collection of high-resolution infrared absorption spectra for a wide range of gases. In this database, absorbance is defined as the logarithm of the ratio of incident to transmitted radiant power through a sample.

The concentrations of these components in the environment can vary widely. For example, absolute humidity typically ranges from <1 % to 5 % by volume. Carbon dioxide concentrations can vary from approximately 400 ppm in outdoor air (Lan et al., 2024) to higher levels indoors, as the carbon dioxide concentration shifts from 0 to approximately 5 % within a single expiratory cycle (Balogh et al., 2016). Ammonia concentrations typically range from ppb levels to several ppm (Li et al., 2020), while methane concentrations can also vary from 1.9 ppm to higher values in outdoor air (Thoning et al., 2022), especially in certain industrial or agricultural settings. It should be considered that other refrigerants may be present, hence propane and R-32 have also been

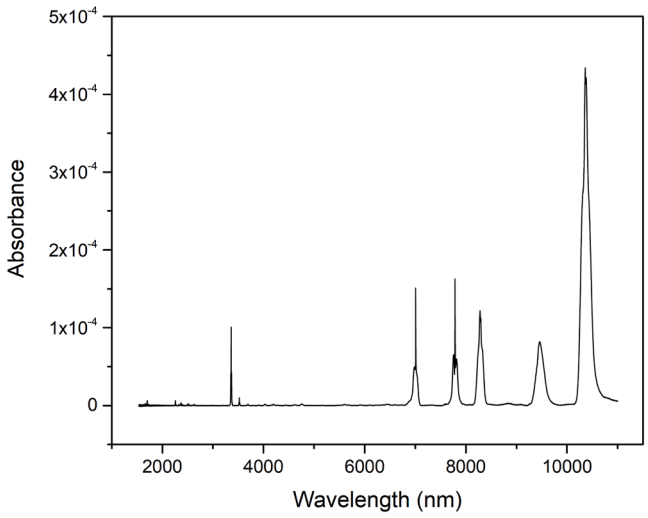

Fig. 2. Absorption spectrum of R-134a in the near and mid-infrared range (PNNL database).

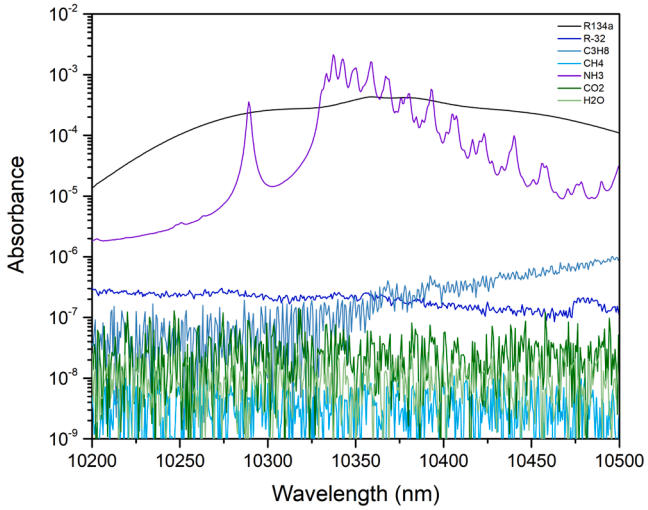

Fig. 3. Absorption spectrum of possible interference components on a logarithmic scale (PNNL database).

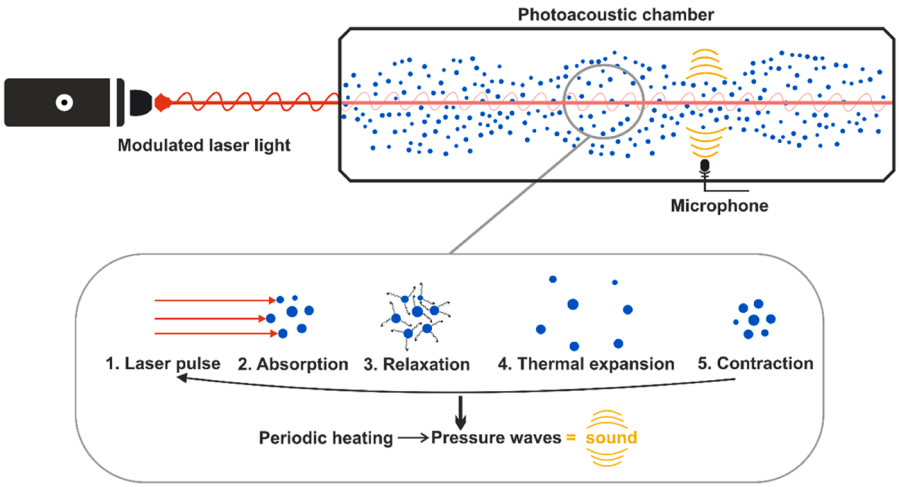

Fig. 1. Schematic diagram of photoacoustic signal generation.

included as possible interference components. Ammonia and carbon dioxide can also be used as refrigerants. (Tian et al., 2009; Zhang et al., 2022)

To accurately determine the spectral interference of other components in the measurement, it is imperative to determine the PA signal that they can generate at their expected concentrations in the environment. Thus, all spectra need to be recorded with the appropriate gas composition.

There are two types of modulation techniques. The amplitude modulation of lasers can be easily accomplished by periodically varying their current between pre-selected values above and below the opening current, so that the laser is switched on and off. The wavelength modulation is achieved by periodically adjusting the laser current to induce slight shifts in the wavelength around the absorption peak. Wavelength modulation can increase the sensitivity, improve stability, and prolong the life of the laser, but it is less effective for detecting large molecules like R-134a, because their absorption spectra exhibit nearly constant, background-like absorption within the narrow adjusting range of the laser. Thus, wavelength modulation is advantageous for molecules with narrow absorption lines, whereas amplitude modulation is more effective for larger molecules, so the latter was used in these measurements. (Hanyecz et al., 2010)

2.5. Experimental setup

The most important parts of the PA system are a laser source, a PA cell, a signal evaluating and controlling electronic unit, and a gas handling system. Figs. 4 and 5 show the schematics of the setup used for the measurements. The light source of the designed measuring system is a QCL (Thorlabs QD10500CM1-AC710) emitting a maximum power of 84 mW within the wavelength range of 10,361 to 10,390 nm. The lasers wavelength is precisely tuned to the peak of the selected absorption line by temperature controlling, while its wavelength is modulated by amplitude modulation, where a square-wave current modulation with a 160 mA amplitude was overlayed on a baseline current of 370 mA. The PA cell is a longitudinal differential cell (Miklós et al., 2001) made of stainless steel, containing two resonator tubes with a 40 mm length and an inner diameter of 3.5 mm each. The PA signal is detected by microphones (SPU0410HR5H-PB, Knowles) positioned at the center of the resonator tubes, where the standing acoustic wave amplitude reaches its maximum. The detected microphone signal is processed by the electronic control unit, which evaluates and amplifies it, then calculates the PA signal using the lock-in detection technique, where the sampling frequency was 50 kHz. The electronic control unit is also used to control temperature sensitive components, such as the laser (33.00±0.001 °C) and the temperature of the PA cell (50.0 ± 0.1 °C). All of the measurements were carried out at atmospheric pressure. The gas handling system was different during the calibration and leak test phases, details are given in the following sections (3.3 and 3.4).

2.6. Calibration

Calibration is the experimental determination of the PA system's sensitivity (Bozóki et al., 2011). The system was calibrated using a conventional approach by measuring the photoacoustic signal in gas mixtures with varying concentrations of R-134a in nitrogen. The concentration of R-134a ranged from 0 to 75 ppm in four steps. To generate concentration variations, pure nitrogen was incrementally substituted with a gas mixture from a cylinder containing nitrogen and 100 ppm of R-134a. By adjusting the flow ratios between the pure nitrogen and the nitrogen enriched with R-134a, four distinct R-134a concentration levels were obtained, consisting of zero concentration and three higher values.

Mass flow controllers (Brooks 5850 s, Brooks Instruments) are used to control gas flows, maintaining a total volumetric flow rate through the PA cell of approximately 100 sccm ($cm^3 \cdot min^{-1}$). While the exact value of this total flow rate does not impact measurement accuracy, the ratio of individual flow rates is crucial for reliable results. Therefore, an absolute flow meter (ADM Flow Meter G6691A, Agilent) with an accuracy of around 2 % was used to calibrate the flow controllers prior to conducting PA measurements.

2.7. Concentration measurement in closed space

The concentration of R-134a gas was measured in a closed box (see

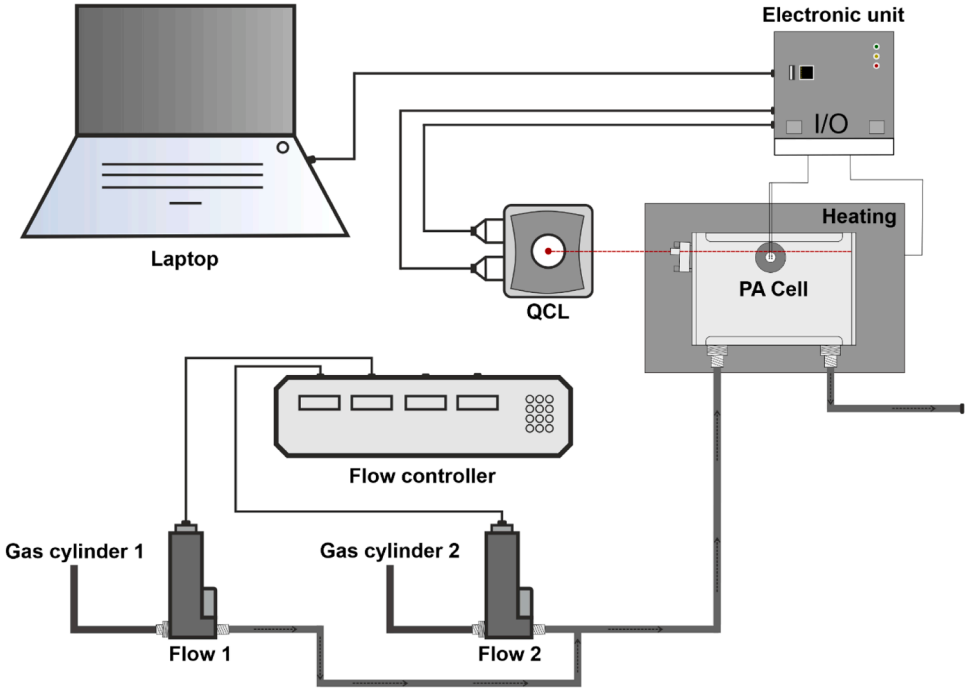

Fig. 4. Schematics of the experimental arrangement used for calibration. The PA system contains a PA cell with a microphone, a quantum cascade laser (QCL), control and signal-processing electronics, and a computer. The gas handling system contains two mass flow controllers.

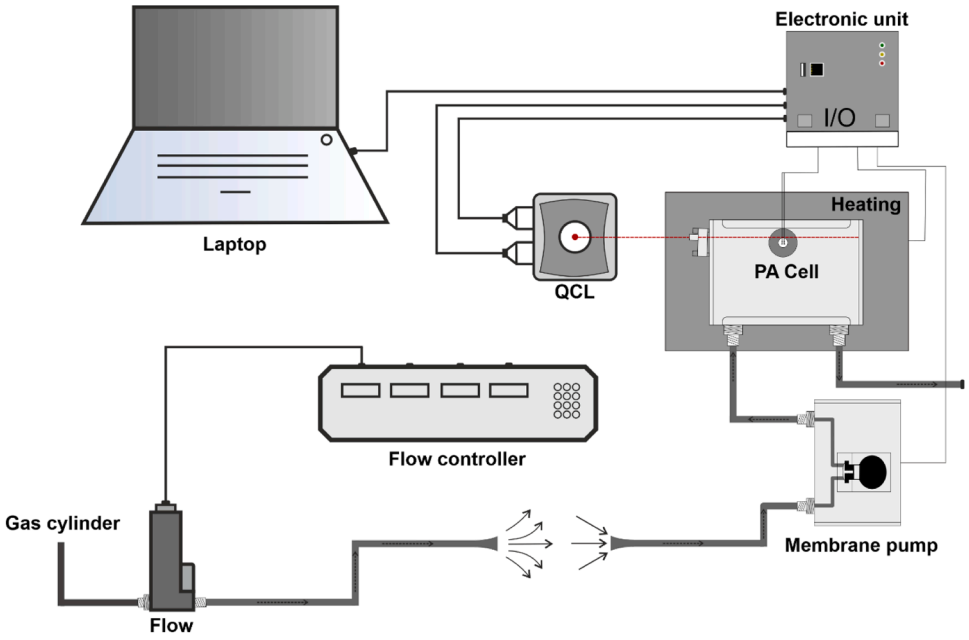

Fig. 5. Schematics of the experimental arrangement used for the leak test.

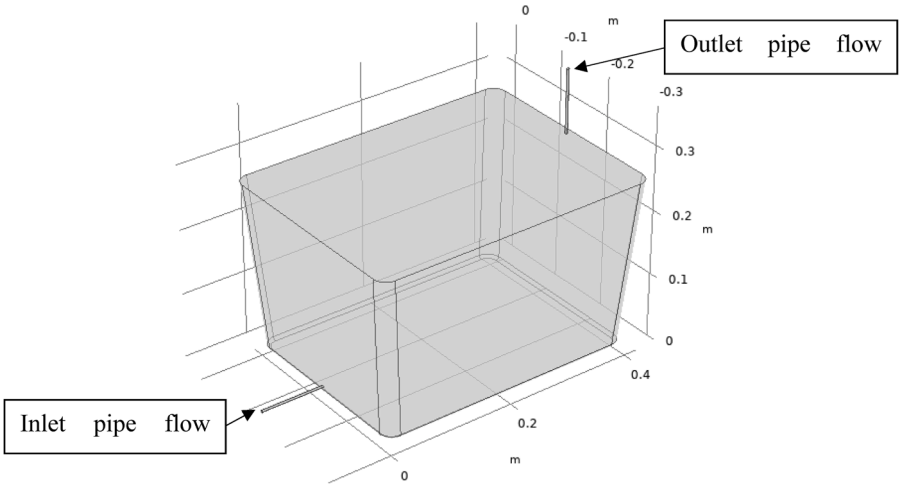

Fig. 6. Geometry of the closed box with inlet and outlet flow fields.

Fig. 6), equipped with inlet and outlet pipes, each having a diameter of 4 mm. The box initially was filled with air and the input gas was a mixture of pure nitrogen and nitrogen containing 100 ppm of R-134a. This mixture was adjusted to produce a total flow of 150 sccm N2 containing 10 ppm of R-134a. In the experimental setup, a membrane pump was used to sample gas from the box through the outlet pipe at the same rate as the inlet flow, ensuring a balanced system. The goal was to monitor the increase in the concentration of R-134a within the box over time. The measurement process involved continuously recording the concentration of R-134a in the box for a duration of 5400 s.

2.8. Leak test

Gas concentration measurements of R-134a were performed using simulated leaks. The controlled release of R134a was achieved using a mass flow controller. The gas that flowed through was nitrogen containing 100 ppm of R-134a at different flow rates. The purpose of these measurements was to detect the presence of leakage, indicated by an increase in the photoacoustic signal. Sampling was performed using a membrane pump at a continuous sampling flow rate between 100–150 sccm, and measurement was conducted as if simulating a real leak detection scenario. The sampling tube was slowly moved at a height of approximately 1 cm above the leak hole, starting at a distance of 10 cm from the leakage point.

3. COMSOL multiphysics simulations

In order to evaluate the accuracy of the R-134a gas concentration leak measurements by a photoacoustic instrument, a detailed, finite element model has been developed and implemented in COMSOL Multiphysics 6.2. First of all, the flow field of the closed box with inlet and outlet pipes with diameters of 4 mm was built up in the finite-element software (see Fig. 6).

Two distinct physical processes (Laminar flow and Transport of Concentrated Species) have been defined and coupled to multiphysics simulation to describe the flow and development of the gas concentration of R-134a at the outlet pipe:

1. Laminar flow: based on preliminary calculations the velocity maximum of the flow is less, than 0.3 m/s, so incompressible laminar flow (Navier-Stokes equation) has been selected from the available Fluid Flow alternatives. As initial conditions, all three velocity components and the relative pressure have been set to zero. Regarding the boundary conditions, most of the external boundaries have been defined as wall (no slip condition), except the inlet and outlet boundaries, where the measured flow rates have been entered and the outlet relative pressure has been set to zero.
2. Transport of Concentrated Species: After the definition of the convection, diffusion had to be added to the simulation. The Fick's law has been selected as diffusion model. All the three materials (R-134a dissolved in nitrogen and air) have been defined by their material parameters (molar masses and diffusion coefficients). As an initial condition, the mass fractions were established: the mass fractions of R-134a and nitrogen were zero and the mass fraction of air in the closed box was 1. Regarding the boundary conditions most of the external boundaries have been defined as no flux, at the inlet boundary the composition of the inlet gas has been entered (concentration of R-134a was 100 ppm dissolved in nitrogen) and as the outflow the outlet boundary has been selected.

After the implementation of the multiphysics model, a physics-controlled mesh has been generated by the internal algorithm of the finite element software (see Fig. 7). The complete mesh consisted of 679,519 domain elements; as a later step, the mesh independence of the results has been checked as well. As a last step, a time-dependent study has been defined from 0 to 5400 s based on the time length of the measurement in question.

After the simulation and the measurements in the small, closed box, we extended the simulation to a much larger scale to investigate how the distribution of the R-134a would behave in a real-world scenario over a larger area. In the extended simulations, the same parameters, conditions, and physics were defined as in the previous one. The extended simulation was conducted within a 5 × 4 × 3 m room, where R-134a gas leaks through a small pipe for 10 h. The mass flow rate was established at 5 g/year, consistent with the maximum allowable leak rate according to regulatory standards. Due to mesh problems with the original 4 mm pipe diameter, it was necessary to increase the diameter to 10 mm to ensure accurate and stable results. This adjustment did not affect the integrity of the physical models or the underlying assumptions but was essential to avoid calculation errors. Within the simulation, six

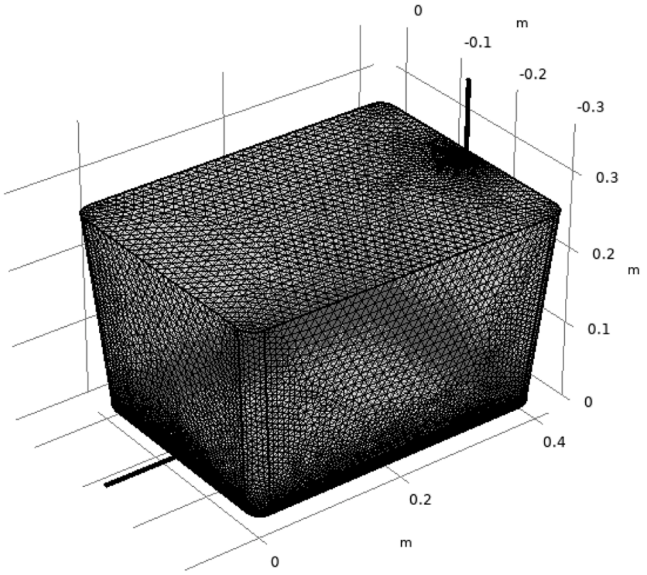

Fig. 7. The generated mesh.

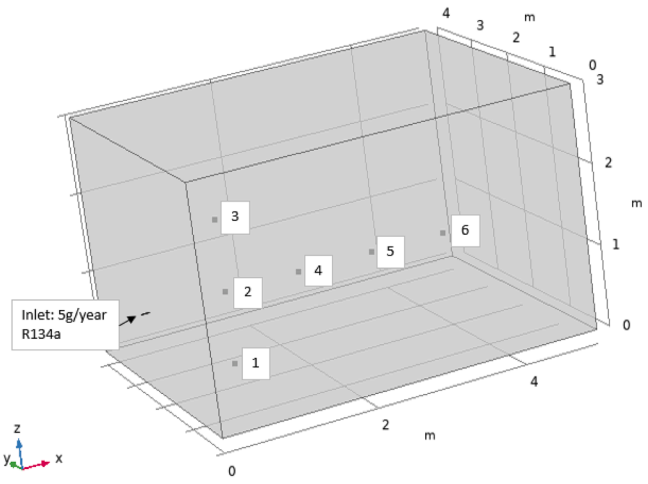

Fig. 8. Geometry of the larger room and the observation points.

observation points were established in the room. These points were used to monitor and track the increase in concentration of R-134a gas over time, the coordinates of the observation points can be seen in Table 1.

4. Results and discussion

This section includes four topics. Section 5.1. covers the process of determining the spectral interference of various gas components and selecting the optimal measurement wavelength and modulation frequency for the following measurements. Section 5.2. details the calibration of the system for the detection of R-134a and the calculation of the minimum detectable concentration. Section 5.3. presents the results of the measurement in closed space and the simulation, followed by a comparison between the two, which highlights the accuracy of the R-134a gas concentration leak measurements. Finally, Section 5.4. outlines the results of measurements conducted near a leak, highlighting concentration changes and their implications in that specific context.

4.1. Spectral interference

To determine the spectral interference of other components with the expected concentrations, spectra were recorded with the following compositions: 4 % water vapor buffered in N_2; 5 % CO_2 buffered in N_2; 5 ppm NH_3 buffered in N_2; 100 ppm CH_4 buffered in synthetic air and 100 ppm R-32 buffered in N_2. The concentration of water vapor can be established by saturating the nitrogen gas stream with water at room temperature, achieved by passing the gas through a water-filled gas scrubber (Hanyecz et al., 2010) Spectral interference can be avoided by carefully choosing the measurement wavelength, i.e., by selecting an absorption band that is not excessively combined with other components of the gas mixture. To maximise the PA signal, the modulation frequency of the laser should be adjusted to align with the resonance frequency of the first longitudinal acoustic resonance of the PA cell. The frequency scan can be carried out near the PA cell's resonance frequency, which can be determined from the maximum response and

Table 1
The coordinates of the main points.

	x (m)	y (m)	z (m)
Inlet	0	2	1
Point 1	1	2	0,1
Point 2	1	2	1
Point 3	1	2	1,9
Point 4	2	2	1
Point 5	3	2	1
Point 6	4	2	1

subsequently used as the modulation frequency for the PA measurement (Szakáll et al., 2009). Therefore, before the spectra were recorded, the first longitudinal resonance of the cell was measured in each gas mixture and a Lorentzian distribution was fitted to extract the resonance frequency (see Fig. 9).

The wavelength of the laser was tuned by tuning its temperature in the range from 10 to 35 °C. R-134a has broad absorption bands within the laser operation wavelength; therefore, any wavelength could be used for R-134a measurements. In Fig. 10 the laser temperature can be seen on the bottom X-axis and the selected wavelength for the further measurements is indicated by the dashed line. The corresponding wavelength scale shown on the top X-axis was fitted to the measured absorption lines according to the PNNL and HITRAN databases. In this case, the wavelength corresponding to $t = 33.00$ °C was chosen for further measurements.

4.2. Calibration

The system was calibrated using a conventional approach in which the concentration of R-134a was changed and then the PA signal was recorded. The system's sensitivity can be quantified by calculating the slope of the line fitted to the data points representing the photoacoustic signals as a function of the corresponding concentrations (see Fig. 11).

The minimum detectable concentration (MDC) was determined by taking three times the standard deviation (3σ) of the measured signal and dividing it by the sensitivity, represented by the slope (m) of the calibration line, in accordance with the IUPAC regulation:

$$MDC = \frac{3\sigma}{m} \tag{3}$$

The standard deviation (σ) of the photoacoustic signal was measured while the concentration of R-134a was zero in the photoacoustic cell and its value was 165 nV. The slope of the R-134a calibration line was evaluated by linear regression, and this slope in units of 6636 nV/ppm corresponds to the sensitivity of the PA system. Based on these parameters, a detection limit of 0.07 ppm of R-134a in nitrogen with an average laser power of 84 mW has been achieved.

4.3. Concentration measurement in closed space and simulation

We conducted a measure to observe how the concentration changes over time. Furthermore, we performed a simulation to evaluate whether it produces results consistent with the experimental measurements, this was essential to ensure that the simulation can be reliably applied to larger spaces, providing estimates of gas concentration levels and detection times.

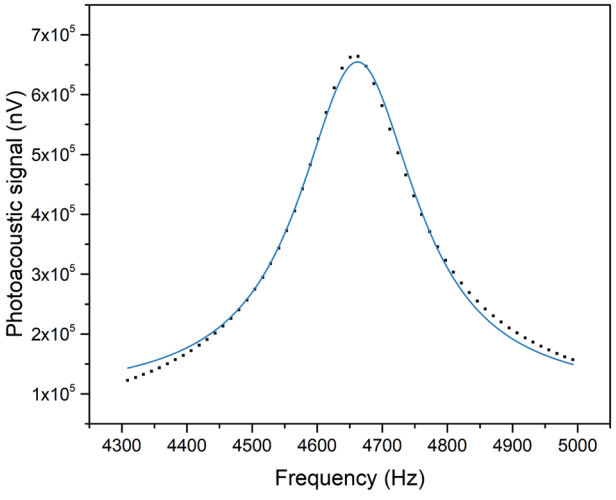

Fig. 9. The black squares represent the measured photoacoustic signals, and the blue line represents the Lorentzian distribution fitted to these data points.

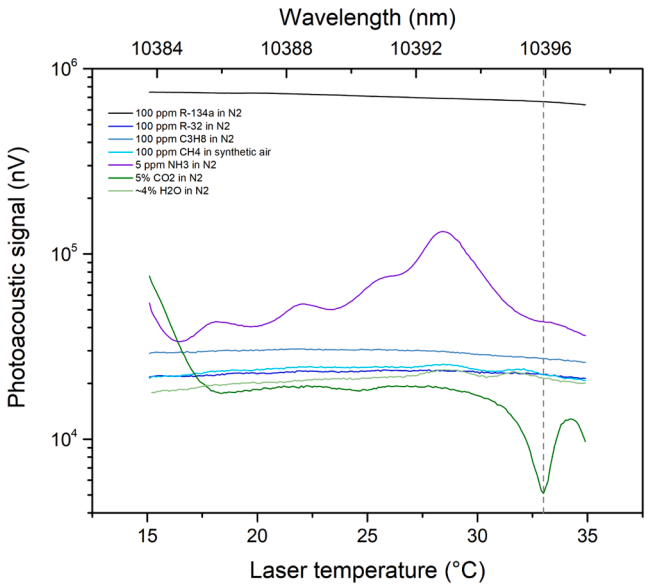

Fig. 10. Absorption cross-sections: PA signal as a function of the laser temperature in different gas compositions on a logarithmic scale.

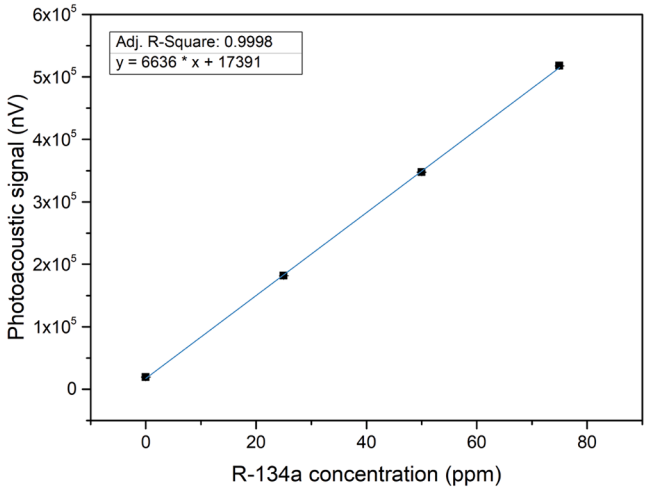

Fig. 11. The measured photoacoustic signal as a function of R-134a concentration in N_2.

After the computation of the time-dependent study the following results have been obtained:

- velocity field in slices of the closed box and streamlines at the last computation time step (see Fig. 12)
- distribution of the mole fraction of R-134a (see Fig. 13) at time step 5400 s.
- and finally, the concentration of the R-134a gas at the outlet boundary was calculated at each time point and compared to the measurement results (see Fig. 14).

As shown in Fig. 14, there is a good agreement (the relative derivation between the measured and simulated concentration is below 10 %) between the measured and simulated concentrations of R-134a gas at the outlet boundary, confirming the reliability of the instrument. The irregularities in the measured photoacoustic signal may be caused by the fact that a membrane pump was used to sample gas from the box, whose

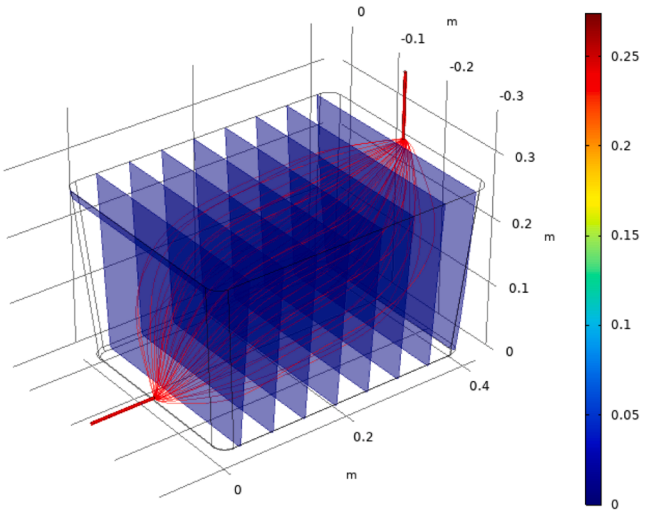

Fig. 12. Velocity field on slices (m/s) and streamlines at time 5400 s.

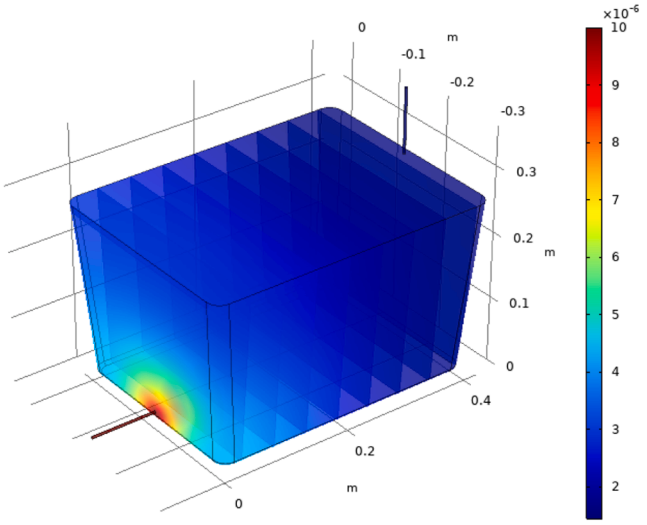

Fig. 13. Mole fraction of R-134a at time 5400 s.

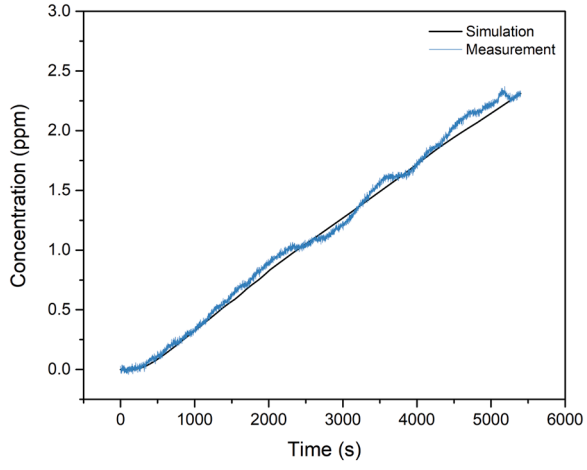

Fig. 14. Measured and simulated concentration of R-134a at outlet.

operation may have fluctuated. Fig. 14 also shows that the initial measured concentration is 0 ppm, meaning that the air components do not cause any measurable cross-effects.

4.4. Simulation in a larger space

The concentrations of R-134a at the observation points were recorded as a function of time and the results were presented on two graphs (Fig. 15 and 16). The first graph shows the increase in concentration at each observation point over time, while the second graph is specifically tied to the detection limit of 0.07 ppm. This second graph allows a better view of the time required at each point for the concentration of R-134a to reach the detectable threshold.

The graph shows that at Point 2 (which is positioned at the same height and one meter away from the inlet), the R-134a concentration increases to a level detectable by the photoacoustic instrument within less than an hour.

As part of the simulation, we generated a series of time-dependent plots representing the surface of the 0.07 ppm concentration front (see Fig. 17). These plots were generated at hourly intervals and provide a clear visual representation of how the detectable concentration isosurface of R-134a evolves in space over time. Because this isosurface moves relatively quickly away from the source of the leak, it can even be detected from a considerable distance within a few hours after the start of the leak.

4.5. Leak detection

We conducted the leak detection test at various flow rates of 100 ppm of R134a buffered in N_2: 5, 10, 20, 50, and 100 sccm, which correspond to flow rates in g/year given in Table 2.

The results show that as the sampling tube approached the leak point, the photoacoustic signal increased, followed by a decrease as it moved away from the leak. This indicates that a sudden increase in the photoacoustic signal suggests that the sampling point is near the leak, as the instrument detects a significantly higher concentration of the refrigerant. Furthermore, we can infer changes in the amount of leakage based on the photoacoustic signal; higher flow rates resulted in larger amplitudes of the photoacoustic signal.

5. Summary and conclusion

The need for reliable and sensitive detection of refrigerant leaks has become increasingly critical due to regulatory bans on refrigerants with high GWP. This article reports on the development of a highly sensitive

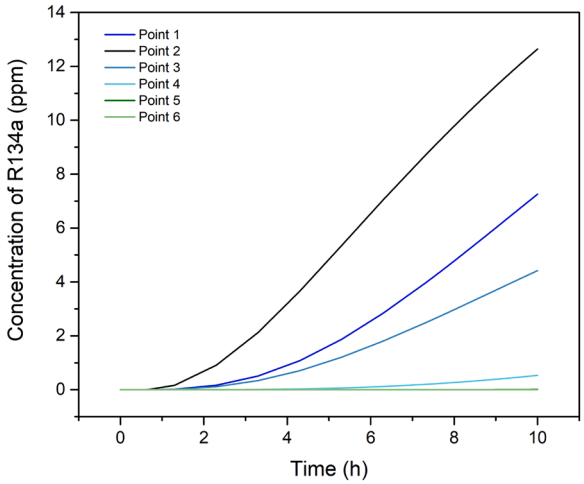

Fig. 15. Concentration increases at each observation point over time.

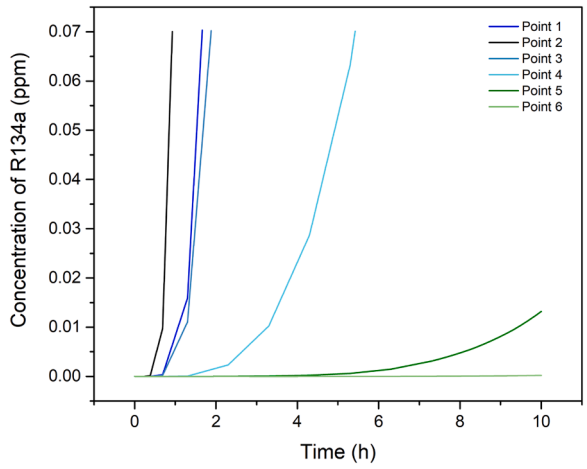

Fig. 16. Concentration increases at each observation point over time.

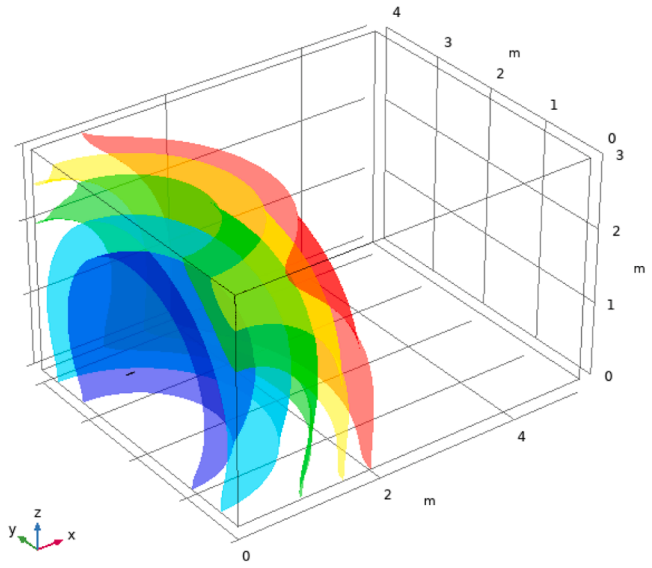

Fig. 17. Evolution of the detectable concentration isosurface over time in two-hour steps: after 2 h (blue), 4 h (turquoise),6 h (green), 8 h (yellow) and 10 h (red).

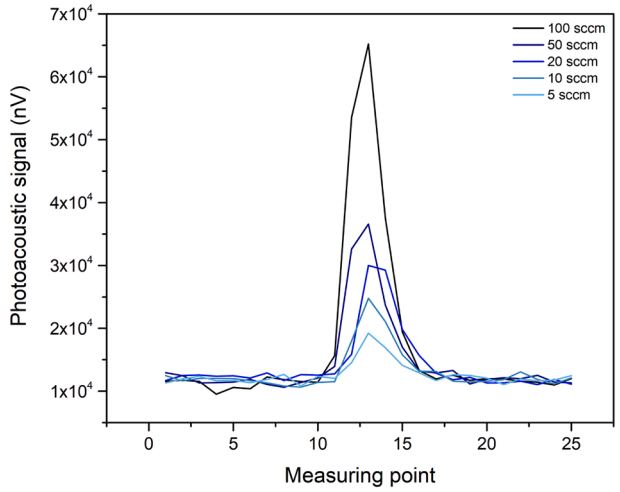

Fig. 18. Demonstration of the variation of the photoacoustic signal near the leakage point for different leakage rates.

Table 2
Flow rates (sccm) used and corresponding leakage values (g/year).

Flow rate of 100 ppm R-134a buffered in N_2 [sccm]	Equivalent flow rate of pure R-134a [g/year]
5	1.20
10	2.39
20	4.79
50	11.97
100	23.93

photoacoustic instrument for the detection and localization of R-134a leaks.

We have successfully developed a photoacoustic instrument capable of detecting R-134a refrigerant, and the following measurements have been made to demonstrate it:

- Measurements in a closed box were carried out to observe changes in R-134a concentration over time, supported by finite element simulations in COMSOL Multiphysics. The simulation outcomes aligned with the experimental observations, confirming the simulation's reliability, thus it was extended to larger environments as well.
- In an extended simulation within a 5 × 4 × 3 m room, we recorded the R-134a concentration at six observation points and generated isosurface plots to visualize the 0.07 ppm concentration front over time. The results demonstrated how quickly the concentration became detectable and highlighted the effectiveness of the instrument in a realistic, larger-scale environment.
- Leak detection tests with controlled releases of R-134a demonstrated the ability of the system to accurately identify leak points and quantify leakage. The fast response time, wide dynamic concentration range, and high sensitivity of the PA instrument make it a promising tool for refrigerant leak detection.

This article also discusses spectral interference from other environmental gases and refrigerants, such as water vapor, carbon dioxide, ammonia, methane, propane, and R-32. By selecting appropriate wavelengths and modulation parameters, the PA system can selectively measure R-134a without false alarms from other components.

To ensure compliance with the requirements of the F-Gas Regulation, a leak detector must have a sensitivity capable of detecting leaks at the maximum allowable rate of 5 g/year. The sensitivity of commercially available refrigerant leak detectors generally varies, but most modern devices can detect refrigerant concentrations at a leak rate of 3–5 g/year. The developed photoacoustic instrument has a significantly higher sensitivity, as demonstrated by the measurements showing its capability to detect leaks at rates as low as 1.2 g/year. In conclusion, this high sensitivity ensures that even the smallest leaks can be reliably detected, providing a more accurate monitoring solution for refrigeration systems.

While this article focused on the detection of R134a, the methodology is adaptable to other refrigerants by utilizing the same principle. With appropriate modifications, such as adjustments to measurement wavelength and detection configuration, the technology can be tailored to detect the presence of alternative refrigerants. The current instrument was specifically assembled for initial laboratory measurements to assess the feasibility of using photoacoustics for refrigerant gas detection. Nevertheless, the setup is fully capable of on-site measurements, featuring an extendable sampling probe that enables sampling from multiple locations without repositioning the main unit. Future development efforts are focused on reducing the instrument's size, and additional measurements are already underway for other gases and for these cases, the instrument design is being optimized to achieve a compact, backpack-sized system, significantly enhancing its portability for field use. The cost of the photoacoustic detection instrument described here mostly depends on the choice of light source. High-power lasers offer greater sensitivity and lower detection limits but come at a

higher cost. This modularity in component selection enables the customization of the instrument to balance performance and budget requirements, making it a versatile tool for a range of applications.

CRediT authorship contribution statement

Panna Végh: Writing – original draft, Visualization, Methodology, Investigation, Conceptualization. **Bence Molnár:** Visualization, Software. **Máté Molnár:** Visualization, Investigation. **Piroska Ailer:** Visualization, Methodology. **Zoltán Bozóki:** Supervision, Funding acquisition, Conceptualization. **Helga Huszár:** Writing – review & editing, Supervision, Project administration, Methodology, Conceptualization.

Declaration of competing interest

The authors declare that they have no known competing financial interests or personal relationships that could have appeared to influence the work reported in this paper.

Acknowledgement

The work was a part of the project „Development of an instrument for the photoacoustic detection of chlorofluorocarbons" project number *ÉZFF/136/2022_TIM_SZERZ*.

Project no 2022–2.1.1-NL-2022–00012 has been implemented with the support provided by the Ministry of Culture and Innovation of Hungary from the National Research, Development and Innovation Fund, financed under the 2022–2.1.1-NL funding scheme.

References

Balogh, A.L., Petak, F., Fodor, G.H., Tolnai, J., Csorba, Z., Babik, B., 2016. Capnogram slope and ventilation dead space parameters: comparison of mainstream and sidestream techniques. Br. J. Anaesth. 117, 109–117. https://doi.org/10.1093/bja/aew127.

Bozóki, Z., Pogány, A., Szabó, G., 2011. Photoacoustic Instruments for Practical Applications: Present, Potentials, and Future Challenges. Appl. Spectrosc. Rev. 46, 1–37. https://doi.org/10.1080/05704928.2010.520178.

Chen, K., Chen, Y., Zhang, B., Mei, L., Guo, M., Deng, H., Liu, S., Ma, F., Gong, Z., Yu, Q., 2020. Highly Sensitive Photoacoustic Microcavity Gas Sensor for Leak Detection. Sensors 20, 1164. https://doi.org/10.3390/s20041164.

Chen, K., Cui, D., Qi, H., Yang, L., Zhao, X., 2024. Multi-component Freon gas detection based on infrared tunable Fabry-Perot detector. Sensors and Actuators B: Chemical 420, 136488. https://doi.org/10.1016/j.snb.2024.136488.

El-Safoury, M., Weber, C., Kiesewetter, O., Hespos, Y., Eberhardt, A., Schmitt, K., Wöllenstein, J., 2020. Miniaturized photoacoustic detection of organofluorine-based refrigerants. J. Sens. Sens. Syst. 9, 89–97. https://doi.org/10.5194/jsss-9-89-2020.

Goebel, D.M., Katz, I., 2008. Gas Flow Unit Conversions and Cathode Pressure Estimates. Fundamentals of Electric Propulsion. Ion and Hall Thrusters, JPL Space Science & Technology Book Series.

Hanyecz, V., Mohácsi, A., Pogány, A., Varga, A., Bozóki, Z., Kovács, I., Szabó, G., 2010. Multi-component photoacoustic gas analyzer for industrial applications. Vib. Spectrosc. 52, 63–68. https://doi.org/10.1016/j.vibspec.2009.10.004.

Heredia-Aricapa, Y., Belman-Flores, J.M., Mota-Babiloni, A., Serrano-Arellano, J., García-Pabón, J.J., 2020. Overview of low GWP mixtures for the replacement of HFC refrigerants: r134a, R404A and R410A. International Journal of Refrigeration 111, 113–123. https://doi.org/10.1016/j.ijrefrig.2019.11.012.

IPCC, 2023. Climate Change 2022 - Mitigation of Climate Change. Working Group III Contribution to the Sixth Assessment Report of the Intergovernmental Panel On Climate Change. Cambridge University Press. https://doi.org/10.1017/9781009157926, 1st ed.

Li, M., Weschler, C.J., Bekö, G., Wargocki, P., Lucic, G., Williams, J., 2020. Human Ammonia Emission Rates under Various Indoor Environmental Conditions. Environ. Sci. Technol. 54, 5419–5428. https://doi.org/10.1021/acs.est.0c00094.

Miklós, A., Hess, P., Bozóki, Z., 2001. Application of acoustic resonators in photoacoustic trace gas analysis and metrology. Review of Scientific Instruments 72, 1937–1955. https://doi.org/10.1063/1.1353198.

Montzka, S.A., McFarland, M., Andersen, S.O., Miller, B.R., Fahey, D.W., Hall, B.D., Hu, L., Siso, C., Elkins, J.W., 2015. Recent Trends in Global Emissions of Hydrochlorofluorocarbons and Hydrofluorocarbons: Reflecting on the 2007 Adjustments to the Montreal Protocol. J. Phys. Chem. A 119, 4439–4449. https://doi.org/10.1021/jp5097376.

Montzka, S.A., Myers, R.C., Butler, J.H., Elkins, J.W., Lock, L.T., Clarke, A.D., Goldstein, A.H., 1996. Observations of HFC-134a in the remote troposphere. Geophys. Res. Lett. 23, 169–172. https://doi.org/10.1029/95GL03590.

Pereira, P.D.V., Melo, C., 2019. A methodology to measure the rates of air infiltration into refrigerated compartments. International Journal of Refrigeration 97, 88–96. https://doi.org/10.1016/j.ijrefrig.2018.08.024.

Qi, H., Xu, Y., Yang, L., Zhao, X., Li, C., Guo, M., Chen, K., 2023. Detection of gaseous halocarbon refrigerants and extinguishing agent based on photoacoustic spectroscopy. Sensors and Actuators B: Chemical 394, 134337. https://doi.org/10.1016/j.snb.2023.134337.

Rivett, A.C., Martin, D., Nickless, G., Simmonds, P.G., O'Doherty, S.J., Gray, D.J., Shallcross, D.E., 2003. In situ gas chromatographic measurements of halocarbons in an urban environment. Atmos. Environ. 37, 2221–2235. https://doi.org/10.1016/S1352-2310(03)00148-1.

Szakáll, M., Varga, A., Pogány, A., Bozóki, Z., Szabó, G., 2009. Novel resonance profiling and tracking method for photoacoustic measurements. Applied Physics B: Lasers and Optics 94, 691–698. https://doi.org/10.1007/s00340-009-3391-5.

Tam, A.C., 1986. Applications of photoacoustic sensing techniques. Rev. Mod. Phys. 58, 381–431. https://doi.org/10.1103/RevModPhys.58.381.

Thoning, K., Dlugokencky, E., Lan, X., 2022. Trends in Globally-Averaged CH4, N2O, and SF6. NOAA Global Monitoring Laboratory. https://doi.org/10.15138/P8XG-AA10.

Tian, H., Yang, Z., Li, M., Ma, Y., 2009. Research and application of CO2 refrigeration and heat pump cycle. Sci. China Ser. E-Technol. Sci. 52, 1563–1575. https://doi.org/10.1007/s11431-009-0175-4.

Végh, P., Gulyás, G., Huszár, H., Ajtai, T., Szabó, G., Szabó, A., Bozóki, Z., 2024. Compensation of composition variation-induced sensitivity changes in gas phase photoacoustics. Infrared. Phys. Technol. 137, 105116. https://doi.org/10.1016/j.infrared.2023.105116.

Zhang, Y., Yang, Z., Lv, Z., Chen, Y., He, H., Chen, S., Liu, B., 2022. Research on the effect of flame retardants on the mildly flammable refrigerant ammonia. J. Loss. Prev. Process. Ind. 77, 104787. https://doi.org/10.1016/j.jlp.2022.104787.